

Manipulation and Real-Time Electrical Detection of Individual Bacterial Cells at Electrode Junctions: A Model for Assembly of Nanoscale Biosystems

Joseph D. Beck, Lu Shang, Matthew S. Marcus, and Robert J. Hamers*

Department of Chemistry, University of Wisconsin, 1101 University Avenue,
Madison, Wisconsin 53706

Received December 22, 2004; Revised Manuscript Received February 23, 2005

ABSTRACT

Biological cells are complex objects that have the potential to act as templates for the subsequent construction of nanoscale structures. We demonstrate the ability to controllably and reversibly manipulate individual, live bacterial cells across micron-sized electrical gaps, and to detect bridging directly through changes in the electrical response. Our model system, *Bacillus mycooides*, is a rod-shaped bacterium approximately 800 nm wide and 5 μm long, similar in size and shape to many inorganic nanowires.

One of the great challenges of nanotechnology remains the assembly of nanoscale objects into more complex systems.^{1–6} The use of hierarchical assembly, in which nanosized objects of arbitrary complexity are fabricated first, and then assembled into functional systems, represents one promising pathway. Biological cells are highly complex objects that have the potential to act as templates for the construction of nanoscale structures and for nanoscale bioelectronic systems.

The dielectrophoretic effect has long been used to manipulate larger cells (typically 10–50 μm in diameter), such as protoplasts, yeast, and eukaryotes.^{7–10} In the dielectrophoretic effect, a nonuniform electric field induces a polarization in the particles of interest; if these particles are more polarizable than the surrounding medium (positive dielectrophoresis), they will move into the region of highest field.¹¹ Previous studies of cells have typically used negative dielectrophoresis, in which cells are repelled by regions of high electric field in solution, to concentrate and/or separate different cell types. However, a number of recent studies have determined that positive dielectrophoresis can be used to manipulate objects such as nanowires and carbon nanotubes, providing one approach for assembly of nanoscale structures.^{4,12,13}

The real-time electrical detection of dielectrophoretic assembly would provide a robust method for fabrication of nanoscale structures. Dielectrophoretic manipulation of cells has typically used optical detection,^{9,10,14–17} although some capacitance measurements have been made of cells in solution^{18,19} and of large numbers of cells on electrodes.²⁰

While these previous studies have addressed many important aspects of dielectrophoretic manipulation, the ability to controllably and reproducibly form electrical “junctions” of individual biological cells with real-time electrical detection has not been previously achieved. Here, we demonstrate the ability to controllably and reversibly manipulate individual, live bacterial cells into micron-sized electrical gaps and to detect bridging of individual bacteria directly through changes in the electrical response.

In this study, we use cells of *Bacillus mycooides*.²¹ As shown in Figure 1a, scanning electron microscopy (SEM) images of this bacterium (here, after drying and sputter-coating with a thin layer of gold) reveal a rod-shaped bacterium approximately 5 μm long and slightly less than 1 μm in diameter. The cell consists of an interior region (cytoplasm, cell wall, and cell membrane) \sim 800 nm in diameter surrounded by a capsule consisting primarily of polysaccharides. This overall structure, consisting of a rigid interior coupled with an organic exterior presenting sites that could be used for biomolecular recognition, parallels that of many of the biofunctionalized inorganic structures of recent interest for nanoscale assembly.^{22–27} While smaller bacterial cells exist, we use this species because the cells are large enough to be visible in optical microscopy, thereby allowing the electrical manipulation and real-time detection to be verified directly.

Cultures of *B. mycooides*²¹ were grown on a laboratory shaker at room temperature in Luria-Bertani broth.²⁸ After 16–24 h of growth, these stationary-phase cultures were pelleted by centrifugation at 5000 g for four minutes. Cultures

* Corresponding author. E-mail: rjhamers@wisc.edu.

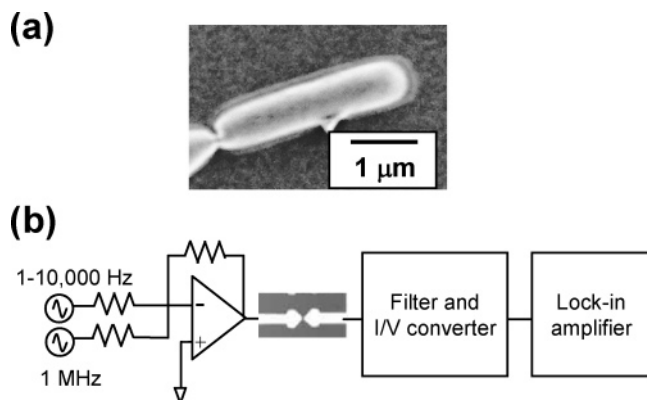


Figure 1. (a) Scanning electron microscope image of a *Bacillus mycooides* after sputter-coating with a thin layer of gold. The bright interior (consisting of the cytoplasm, cell membrane, and cell wall) can be seen, surrounded by a faint halo from the bacterial capsule. (b) Diagram of the equipment setup used in experiments.

were suspended in distilled H₂O, and this wash step was repeated once more. Two mL of washed cells were diluted into 50 mL of 90% H₂O and 10% glycerol for experimental use.

Our assembly consisted of a polyacrylic base, a micro-patterned chip, polydimethylsiloxane (PDMS) mold with hollow chamber, and a transparent coverslip. Gold electrodes were fabricated onto a SiO₂-coated Si wafer using standard optical lithography and evaporation techniques. A hollow 3 × 2 × 1.5 mm chamber was fabricated in PDMS with microfluidic channels for fluid flow. The bottom of the chamber was directly exposed to the micropatterned chip, while the top was exposed to a glass coverslip. This arrangement permitted the bacteria to be directly observed and recorded on a microscope-mounted video camera during electrical manipulation and measurement.

As shown in Figure 1b, we use two simultaneously applied AC potentials: a high-frequency field (~1 MHz) of variable amplitude to manipulate the bacteria, and a second, lower-frequency field (1–10 kHz, ~10 mV) to detect their assembly. These AC potentials were summed in a home-built operational amplifier and applied to one electrode. The other electrode was connected to a custom-built current-to-voltage converter (10⁶ V/amp) with an integrated low-pass filter to reject the high-frequency current while amplifying the low-frequency signals. The amplifier output signal was connected to a lock-in amplifier to synchronously detect the low-frequency current passing through the electrode assembly. Experiments reported were achieved using a 90% water/10% glycerol mixture that was slowly flowed through the assembly at a linear velocity of approximately 0.1 mm/s.

Figure 2a presents selected still frames extracted from a video demonstrating the capture and delivery of cells to an electrode gap. Arrowheads track the fate of one specific bacterium over time as it is transported to the electrode gap. The number in the corner indicates the time (seconds) after this bacterium was caught at the electrode surface. At –5 s, no voltage was applied and cells freely float over the electrodes; most of these are out-of-focus. An AC voltage

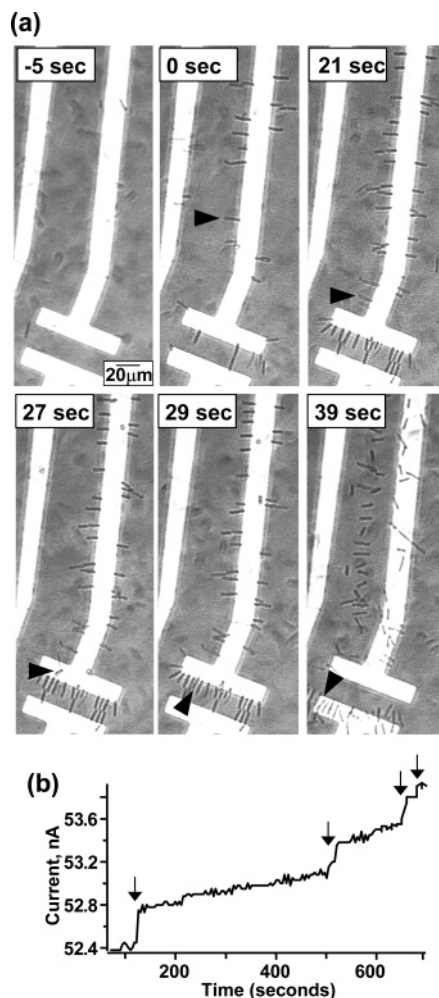


Figure 2. Capture, transport, and detection of bacteria. (a) Arrows track the fate of the same bacterium as it is transported to the electrode gap. The number in the corner represents seconds after this bacterium was caught at the electrode surface. At –5 s, no potential was applied yet. At 0 s, a potential of 1.5 V_{pp} captures bacteria along the electrode. At 21s, 27s, 29s, a 0.5 V_{pp} potential was applied, permitting transport across the electrode surface. Immediately before the 39 s image, the high-frequency voltage was reduced to 10 mV_{pp}, releasing the bacteria. Frequency was 1 MHz at all times. (b) Real-time measurement of bacterial accumulation using a 1 MHz manipulation potential (200 mV_{pp}) and a 1 kHz (20 mV_{pp}) measuring potential. These measurements were performed using electrodes such as those shown in Figure 2a, except with a smaller, 10 micron gap. Times at which a bacterium was microscopically observed entering the electrode gap are marked with an arrow.

of 1.5 V peak-to-peak (V_{pp}) at 1 MHz was then applied; this captures cells at the electrode edges, leading to an accumulation of cells at the edges of the electrode, as shown in the frame at 0 s. At this voltage the cells do not easily move; however, if another cell is captured, the adjacent cells will readjust their positions slightly. When the applied potential is lowered to 0.5 V_{pp}, cells continue to be captured. With a small flow (approximately from top to bottom), the cells are selectively transported downward, where they accumulate in the electrode gap. The frames shown at 21, 27, and 29 s show the directed motion of the cells, which move in a smooth, conveyor-like motion along the wire edge and finally move into the bottom electrode gap. To demonstrate that

the cellular manipulation is reversible, we lowered the applied AC voltage to 10 mV just before the frame at 39 s. This frame shows that the bacteria are released from the electrode and move as free cells in solution. This video is available as Supporting Information.

While only selected frames are reported here, more detailed studies show that there are at least three ranges of behavior. At large voltages ($>2 V_{pp}$), the cells are irreversibly immobilized and there is likely perforation of the cell walls. At intermediate voltages (approximately $0.5\text{--}2.0 V_{pp}$), the bacteria are controllably and reversibly captured and then released by merely lowering the potential sufficiently; cell-staining methods show that the cells remain alive after capture and after release. At even lower voltages ($0.1\text{--}0.5 V_{pp}$), bacteria are captured gently enough that they can be propelled along the electrode surface by liquid flow (Figures 2 and 3). The use of low voltage combined with a small flow leads to the ability to controllably capture individual bacteria and then transport them along the length of the electrode and direct them into a gap between two electrodes. Finally, at voltages of less than $\sim 80\text{ mV}_{pp}$, the cells are released into solution.

We can also directly detect the arrival of the cells electrically. On large electrodes, this detection can be done in an “accumulation” mode in which an increase in current is observed each time a bacterium enters and spans the gap. Figure 2b shows electrical measurements made using electrodes similar to those shown in Figure 2a, but with a smaller ($3.5\ \mu\text{m}$) gap between the electrodes that is small enough such that a single bacterium can completely bridge between electrodes. The electrical measurements (1 kHz , 20 mV_{pp}) show a series of step-like increases. The simultaneous video images (not shown) reveal that there is perfect correlation between the step-like increases and bacterial bridging events.

The above results demonstrate the ability to capture and to detect the manipulation of multiple cells. By decreasing the electrode size and tapering the electrodes to a point, it is possible to capture and electrically characterize *individual* cells, by directing the cells to single point. By turning the 1 MHz manipulation potential on and off, it is possible to operate in a “catch-and-release” mode in which individual bacteria are captured, transported to the electrode gap, characterized electrically, and then released. Figure 3 shows the reversible capture, manipulation, and release of a single cell at teardrop-shaped electrodes with an electrode gap of $3.5\ \mu\text{m}$. The complete video from which these frames were extracted is available in the Supporting Information.

In Figure 3, the panels follow the motion of a single cell, labeled “C1”. At -8 s it is freely floating in solution. After flowing near the energized electrode, it is captured (0 s) and then transported down the length of the electrodes to the end (92 s), around the teardrop-shaped electrode end (119 s), and into the gap (120 s). Again, when the field was released (just before 155 s), the cell was released into solution. The bottom panels show an enlarged version of the image at 120 and 155 s .

To characterize the frequency response of the bacterium, we performed repeated “catch and release” measurements

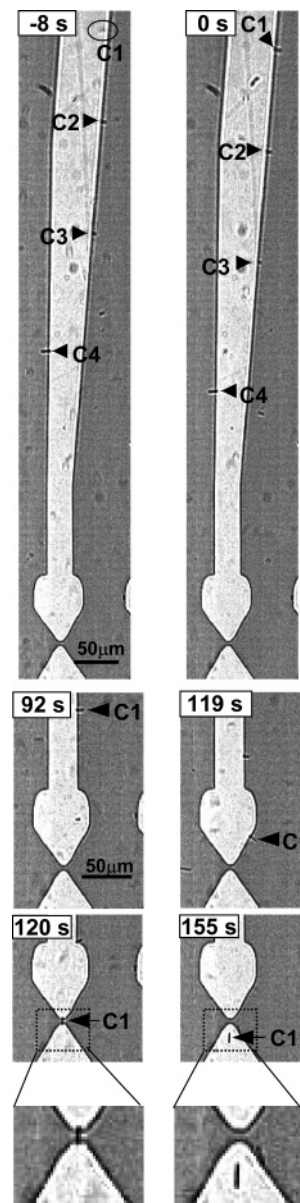


Figure 3. Long distance transport to the interelectrode gap. Arrows (or a circle) track several individual bacteria (labeled C1–C4). The bacterium C1 is tracked as it is captured at the electrode edge (0 s), transported $700\ \mu\text{m}$ to the junction ($0\text{ s} - 119\text{ s}$), and captured across the electrode junction (120 s) where it was held fixed until finally being released (155 s). Numbers correspond to the time (in seconds) after bacterium “C1” was captured. Alignment potential was 1 MHz and 200 mV_{pp} in all panels except at 155 s , where the potential was temporarily lowered to 10 mV_{pp} . The bottom two panels show enlargements of the electrode gap region for the 120 s and 155 s images.

in which we used a constant 1 MHz , 200 mV_{pp} alignment potential and a 20 mV_{pp} measuring potential, and then measured the current as a function of frequency from 10 Hz to 10 kHz just before and just after a bacterium was delivered to the gap. Subtracting these yields the change in current due to the single bacterium bridging the electrodes. Because no statistically significant differences in frequency response were observed between individual bacteria, we averaged the response from seven different bacteria to obtain an averaged frequency response with a higher signal-to-noise ratio, shown

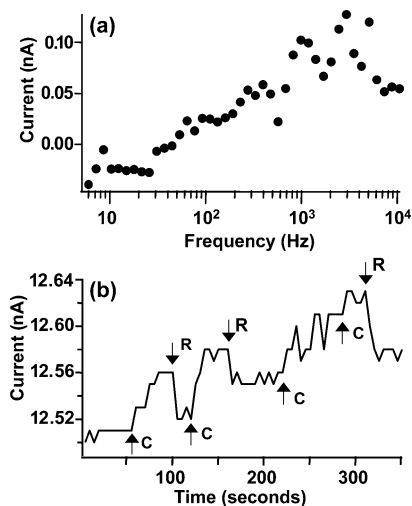


Figure 4. Electrical measurements of bacteria bridging across the teardrop-shaped, 3.5 μm -spacing electrode gaps shown in Figure 3. Bacteria were aligned using a continuous 1 MHz, 200 mV_{pp} potential as in Figure 3. (a) Change in current induced by bridging of bacteria across the gap. This graph is the average of seven frequency spectra, each made on a single bacterium. (b) Real-time change in current at 1 kHz induced by bridging of individual bacteria across the electrode gaps operated in a “catch-and-release” mode. The arrows labeled “C” mark the moment a bacterium is captured between the electrodes. Arrows labeled “R” mark the moment a bacterium is released from the electrode gap by momentarily reducing the 1 MHz potential.

in Figure 4a. This plot shows that at frequencies between 100 Hz and 100 kHz, the bacterium increases the current between the electrodes. At the very lowest frequencies (<100 Hz) the data suggests that the bacterium might yield a slight decrease in current; however, at these low frequencies the change in current from a single bacterium is extremely small, and tests of “real-time” detection at these lowest frequencies were inconclusive. Nevertheless, at frequencies >100 Hz it is clear from the frequency spectra and the real-time measurements that a single bacterium induces a significant increase in the current upon bridging the two electrodes.

The higher sensitivity at higher frequencies observed in Figure 4a suggests that the change in current when a cell bridges the electrode gap arises primarily from the changes in capacitance. Previous studies have reported that cells increase the conductivity of bulk solutions and have attributed this increase to two effects.^{16–18} First, the ionic charges within the cytoplasm can respond to external electric fields, thereby increasing the capacitance.¹⁸ Second, fixed charges within and near the cell wall (especially for gram-positive bacteria such as *B. mycooides*) induce a layer of mobile ions that give cells a surface conductivity and contribute to the capacitance.²⁹ While we have not yet determined which of these factors dominates the overall response for bacterial directly bridging the microelectrodes, the increase in current with increasing frequency indicates that there is some capacitive component to the response. More detailed modeling will be required to fully model the electrical response associated with a single bacterium.

Finally, Figure 4b shows the real-time change in electrical signals accompanying the sequential “catch-and-release”

manipulation of several bacteria. Here, a 1 MHz, 200 mV_{pp} potential was used to manipulate the bacteria, and 1000 Hz, 20 mV_{pp} potential was used for real-time detection. In Figure 4b, the electrode gap is initially empty and the signal arises from capacitive coupling of the bare electrodes in the solution. The manipulation field was applied with a slow fluid flow and a dilute cell solution, causing a single bacterium to bridge the gap. When bridging occurred, there was a sudden increase in current (Figure 4b). After about 30 s, the 1 MHz potential was lowered to 1 mV_{pp} for 1–3 s, which released the bacterium. After release, the current immediately fell to a level comparable to (but slightly higher than) that observed before the bacterial bridging. If a second bacterium was delivered to the gap, an additional increase in current occurred. Again, when the voltage was lowered for 1–3 s (releasing the bacterium), the current decreased to previous levels.

Figure 4b shows that the increase in current due to bacterial bridging is not instantaneous, but instead increases more slowly over a period of ~ 20 s, while the release occurs more quickly and is limited by the time constant of the lock-in amplifier (~ 3 s). In some cases the bacteria do not bridge perfectly and appear to make and break the electrical contact several times (as in the third “capture” even in Figure 4b). We believe that part of this behavior is attributable to the polysaccharide capsule on the bacterium. While the bacterium may come into initial contact with the electrode, there are likely slower changes in the polysaccharide layer that occur over a time span of ~ 20 s that provide improved electrical contact to the electrode surface.

Figure 4b also shows that, over the course of several minutes, there is a steady increase in background current. Control experiments were performed using an identical solution without any bacteria present. These control samples showed a very constant impedance value, demonstrating that the upward drift in background current in Figure 4b is directly associated with the presence of bacteria. Measurements using cell vitality stains (described below) indicate that a small number of cells die during the course of an experiment. We conjecture that the increasing background current likely arises from ions either diffusing out of the large number of healthy cells or from the smaller number of cells that die and release their highly ionic cytoplasm into the glycerol-deionized water mixture used in our measurements.

Finally, we investigated whether the bacteria being manipulated remained alive using two commonly used vitality stains. One stain, propidium iodide, is a hydrophilic molecule that cannot penetrate the hydrophobic cell membrane. However, it can diffuse into cells with perforated membranes, where it binds DNA and creates a red fluorescence. Another cell vitality stain, calcein AM, is hydrophobic, so it can diffuse across intact cell membranes. Calcein-AM is metabolized by the cell into calcein, which binds Ca^{2+} and fluoresces. The presence of intense green fluorescence shows that the cells are alive. Our data on the electrodes used here show that applied potentials of greater than 2 V (at 1 MHz) can induce cell death. However, at the smaller potentials used to manipulate the cells, the vitality stains indicate that the

cells are alive, as indicated by the presence of intact cell walls (no fluorescence from propidium iodide) and by active metabolic processes (intense fluorescence from calcein).

The results shown here are significant because while there has been much attention paid to the ability to manipulate nanoscale objects such as nanotubes and nanowires across electrical contacts, for many applications (such as biological sensing), the use of bacterial cells affords a number of potential advantages. For example, since the external surfaces of cells express specific proteins, the use of cellular manipulation combined with the use of secondary biological interactions such as antibody binding to the cells can potentially be used to create even more complex nanoscale structures. Thus, we believe that bacterial cells can serve as a template for the construction of a wide variety of nanoscale structures. The ability to easily capture, manipulate, and detect the binding of these cells in real time suggests that they may represent a facile pathway for the construction of nanoscale structures, especially those that aim to integrate nanotechnology with biology.

Acknowledgment. The authors acknowledge the assistance of Sarah Baker and Kevin Metz with the SEM imaging. This material is based upon work supported by the National Science Foundation grants DMR-0210806 and DMR-0425880, and by Sensir Technologies.

Supporting Information Available: Videos of the cellular manipulation shown in Figure 2 and Figure 3 are available. This information is available free of charge via the Internet at <http://pubs.acs.org>.

References

- (1) Hermanson, K. D.; Lumsdon, S. O.; Williams, J. P.; Kaler, E. W.; Velev, O. D. *Science* **2001**, *294*, 1082–1086.
- (2) Whang, D.; Jin, S.; Wu, Y.; Lieber, C. M. *Nano Lett.* **2003**, *3*, 1255–1259.
- (3) Cai, L. T.; Skulason, H.; Kushmerick, J. G.; Pollack, S. K.; Naciri, J.; Shashidhar, R.; Allara, D. L.; Mallouk, T. E.; Mayer, T. S. *J. Phys. Chem. B* **2004**, *108*, 2827–2832.
- (4) Smith, P. A.; Nordquist, C. D.; Jackson, T. N.; Mayer, T. S.; Martin, B. R.; Mbindyo, J.; Mallouk, T. E. *Appl. Phys. Lett.* **2000**, *77*, 1399–1401.
- (5) Wu, Y. Y.; Yan, H. Q.; Huang, M.; Messer, B.; Song, J. H.; Yang, P. D. *Chem., Eur. J.* **2002**, *8*, 1261–1268.
- (6) Huang, Y.; Duan, X. F.; Wei, Q. Q.; Lieber, C. M. *Science* **2001**, *291*, 630–633.
- (7) Gascoyne, P. R. C.; Vykoukal, J. V. *Proc. IEEE* **2004**, *92*, 22–42.
- (8) Suehiro, J.; Pethig, R. *J. Phys. D: Appl. Phys.* **1998**, *31*, 3298–3305.
- (9) Talary, M. S.; Burt, J. P. H.; Tame, J. A.; R. Pethig *J. Phys. D: Appl. Phys.* **1996**, *29*, 2198–2203.
- (10) Markx, G. H.; Huang, Y.; Zhou, X.-F.; Pethig, R. *Microbiology* **1994**, *140*, 585–591.
- (11) Pohl, H. A. *Dielectrophoresis: The Behavior of Neutral Matter in Nonuniform Electric Fields*; Cambridge University Press: Cambridge, U. K., 1978.
- (12) Krupke, R.; Hennrich, F.; v. Löhneysen, H.; Kappes, M. M. *Science* **2003**, *301*, 344–347.
- (13) Krupke, R.; Hennrich, F.; Kappes, M. M.; v. Löhneysen, H. *Nano Lett.* **2004**, *4*, 1395–1399.
- (14) Morgan, H.; Hughest, M. P.; Green, N. G. *Biophys. J.* **1999**, *77*, 516–525.
- (15) Markx, G. H.; Talary, M. S.; Pethig, R. *J. Biotechnology* **1994**, *32*, 29–37.
- (16) Pethig, R.; Markx, G. H. *Trends Biotechnol.* **1997**, *15*, 426–432.
- (17) Wang, X.-B.; Huang, Y.; Burt, J. P. H.; Markx, G. H.; Pethig, R. *J. Phys. D: Appl. Phys.* **1993**, *26*, 1278–1285.
- (18) Sohn, L. L.; Saleh, O. A.; Facer, G. R.; Beavis, A. J.; Allan, R. S.; Notterman, D. A. *Proc. Natl. Acad. U.S.A.* **2000**, *97*, 10687–10690.
- (19) Gawad, S.; Schild, L.; Renaud, P. *Lab on a Chip* **2001**, *1*, 76–82.
- (20) Suehiro, J.; Yatsunami, R.; Hamada, R.; Hara, M. *J. Phys. D: Appl. Phys.* **1999**, *32*, 2814–2820.
- (21) Bacillus Genetic Stock Center. ID# 6A11.
- (22) Baker, S. E.; Lasseter, T. L.; Smith, L. M.; Hamers, R. J. *Mater. Res. Soc. Symp. Proc.* **2003**, *F4.6.1*, 737.
- (23) Keren, K.; Berman, R. S.; Buchstab, E.; Sivan, U.; Braun, E. *Science* **2003**, *302*, 1380–1382.
- (24) Wang, J.; Liu, G.; Jan, M. R. *J. Am. Chem. Soc.* **2004**, *126*, 3010–3011.
- (25) Katz, E.; Willner, I. *ChemPhysChem* **2004**, *5*, 1085–1104.
- (26) Hazani, M.; Hennrich, F.; Kappes, M.; Naaman, R.; Peled, D.; Sidorov, V.; Shvarts, D. *Chem. Phys. Lett.* **2004**, *391*, 389–392.
- (27) Maubach, G.; Fritzsche, W. *Nano Lett.* **2004**, *4*, 607–611.
- (28) Luria-Bertani broth consists of 10 g tryptone, 5 g yeast extract, and 5 g NaCl, brought to 1 L volume with water.
- (29) Carstensen, E. L.; Cox, H. A., Jr.; Mercer, W. B.; Natale, L. A. *Biophys. J.* **1965**, *5*, 289–301.

NL047861G